

## **A direct comparison of monomeric vs dimeric and non-annulated vs N-annulated perylene diimide electron acceptors for organic photovoltaics**

Maryam Nazari, Edward Cieplechowicz, Thomas A. Welsh, Gregory C. Welch\*

<sup>a</sup> Department of Chemistry, University of Calgary, 2500 University Drive N.W., Calgary, Alberta, Canada  
T2N 1N4

\* Corresponding Author

Email: gregory.welch@ucalgary.ca

Phone Number: 1-403-210-7603

### **Supporting Information**

#### **TABLE OF CONTENTS**

<b>1.</b>	<b>Materials and Methods</b>	<b>S2</b>
<b>2.</b>	<b>Synthetic Details/Experimental Procedures</b>	<b>S4</b>
<b>3.</b>	<b><sup>1</sup>H and <sup>13</sup>C NMR Spectra</b>	<b>S6</b>
<b>4.</b>	<b>Mass Spectrum</b>	<b>S9</b>
<b>5.</b>	<b>Temperature Dependent Optical Absorption Spectra of Neat Compounds</b>	<b>S10</b>
<b>6.</b>	<b>Photoluminescence Spectra of Neat Compounds</b>	<b>S11</b>
<b>7.</b>	<b>Electrochemistry</b>	<b>S12</b>
<b>8.</b>	<b>Computational Analysis</b>	<b>S15</b>
<b>10.</b>	<b>Optical Absorption and Photoluminescence Spectroscopy of BHJ Films</b>	<b>S17</b>
<b>11.</b>	<b>Organic Solar Cell Data</b>	<b>S18</b>
<b>12.</b>	<b>AFM Height and Phase Images of BHJ Blends</b>	<b>S21</b>
<b>13.</b>	<b>References</b>	<b>S22</b>

# 1. Materials and Methods

**Synthetic methods:** Reactions were carried out in the air or under an inert N<sub>2</sub> atmosphere where indicated. For reactions requiring heat, the reaction vessels were placed in a LabArmor® bead bath heated to the desired temperature.

**Materials:** The palladium homogeneous catalyst, Pd<sub>2</sub>(dba)<sub>3</sub>, was purchased from Oakwood Chemical. All other materials were purchased from Sigma-Aldrich. All solvents and materials purchased were used without further purification. Polymers PTB7-Th (CAL-OS, PCE10, Mw > 100 kg/mol, batch no C-03) and PffBT4T-2OD (1- Material, PCE11, Mw = 100-150 kg/mol, PDI=2.0-2.5, batch no YY8198CB) were purchased and used as received.

**Microwave-Assisted Synthesis:** All microwave reactions were carried out using a Biotage® Initiator+ microwave reactor. The operational power range of the instrument is 0–400 W, using a 2.45 GHz magnetron. Pressurized air is used to cool each reaction after microwave heating.

**Nuclear Magnetic Resonance (NMR):** The reported <sup>1</sup>H and <sup>13</sup>C{H} spectra were acquired on a Bruker Avance 500 MHz spectrometer at 300K. Both <sup>1</sup>H and <sup>13</sup>C are reported in parts per million and performed in deuterated chloroform (CDCl<sub>3</sub>). Multiplicities are reported as singlet (s), doublet (d), triplet (t), quartet (q), and multiplet (m).

**High-resolution mass spectrometry (HRMS):** High-resolution MALDI mass spectrometry measurements were performed courtesy of Jian Jun (Johnson) Li in the Chemical Instrumentation Facility at the University of Calgary. A Bruker Autoflex III Smartbeam MALDI-TOF (Na:YAG laser, 355 nm), setting in a positive reflective mode, was used to acquire spectra. Operation settings were all typical, e.g., laser offset 62–69; laser frequency 200 Hz; and a number of shots 300. The target used was Bruker MTP 384 ground steel plate target. The sample solution (~ 1 µg/ml in dichloromethane) was mixed with matrix trans-2-[3-(4-tert-Butylphenyl)-2-methyl-2-propenylidene]malononitrile (DCTB) solution (~ 5 mg/ml in methanol), pipetted 1 µl solution above to target spot and dried in the fume hood.

**Cyclic Voltammetry (CV):** Electrochemical measurements were performed using a Model 1200B Series Handheld Potentiostat by CH Instruments Inc. The instrument used a standard three electrode configuration: Ag/Ag<sup>+</sup> pseudo-reference electrode, platinum wire counter electrode, and glassy carbon working electrode. Experiments were performed in anhydrous dichloromethane, which was degassed with a nitrogen gas purge for 10 minutes. Tetrabutylammonium hexafluorophosphate (TBAPF<sub>6</sub>) was used as the supporting electrolyte at a concentration of ~0.1 M. The samples were scanned at 100 mV/s. Sample concentration was ~0.4 mg/mL. Estimations of the energy levels were obtained by correlating the E<sub>1/2</sub> values of oxidation and first reduction to the normal hydrogen electrode (NHE), assuming an IP energy of 4.80 eV for Fc/Fc<sup>+</sup>;

$$\text{HOMO} = -(E_{1/2 \text{ ox}} + 4.80)$$

$$\text{LUMO} = -(E_{1/2 \text{ red}} + 4.80)$$

**UV-Visible Spectroscopy (UV/vis):** Absorption measurements of neat compounds and blended films were performed using an Agilent Technologies Cary 60 UV-vis spectrometer at room temperature, and elevated

temperature measurements were heated via Peltier heating unit. All solution UV/vis experiments were run in chlorobenzene (C<sub>6</sub>H<sub>5</sub>Cl) using 2 mm quartz cuvettes and diluted to 0.01 mg/mL solutions. Thin-films of neat compounds were prepared by spin-coating 10 mg/mL solutions from C<sub>6</sub>H<sub>5</sub>Cl onto Corning glass micro slides at 1500 rpm. Blends films were prepared as detailed in section 11. Prior to use, glass slides were cleaned with soap and water, acetone and isopropanol, and followed by UV/ozone treatment using a Novascan UV/ozone cleaning system.

**Photoluminescence (PL):** All emission measurements of neat compounds and blended films were recorded using an Agilent Technologies Cary Eclipse fluorescence spectrophotometer at room temperature. Solutions used C<sub>6</sub>H<sub>5</sub>Cl as the solvent while all neat films were prepared by spin-coating 10 mg/mL solutions from C<sub>6</sub>H<sub>5</sub>Cl onto Corning glass micro slides at 1500 rpm. Blends films were prepared as detailed in section 11.

**Determination of photoluminescence quantum yield (QY):** The photoluminescence quantum yield (PL QY) of the compounds **1**, **2**, **3**, and **4** in C<sub>6</sub>H<sub>5</sub>Cl were estimated by using the comparative method proposed by Williams et. al. (A. T. R. Williams, S. A. Winfield, J. N. Miller, *Analyst* 1983, 108, 1067) after slight modification as follows:

$$Q_X = Q_R \frac{A_R F_X}{A_X F_R} \left( \frac{n_X}{n_R} \right)^2$$

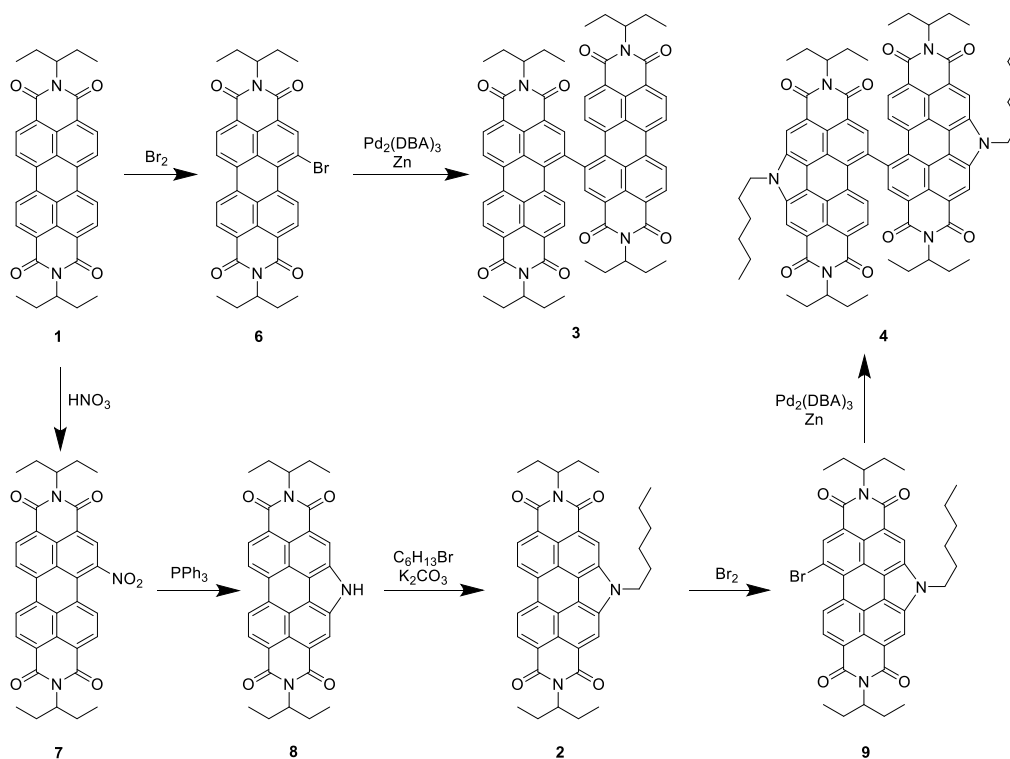
where Q is the PL QY, A is the absorbance of the solution, F is the corrected PL emission intensity, and n is the average refractive index of the solution. Subscripts R and X refer to the standard selected and acceptor compounds, respectively. Rhodamine B (Sigma-Aldrich Co., St Louis, MO, USA) is used as the standard for the PL QY calculation. To minimize reabsorption effects, the absorbance values of the standard and acceptor compounds were controlled to be less than 0.1 at the respective excitation wavelengths. We chose 490 nm as the excitation wavelength for Rhodamine B and PDI acceptors.

**Atomic Force Microscopy (AFM):** AFM measurements were performed by using a TT2- AFM (AFM Workshop) in tapping mode and WSxM software with a resonance frequency of 300 kHz, a force constant of 40 N/m and a reflective back side aluminum coating (Tap300Al-G, BudgetSensors). Samples for AFM measurements were the same ones that were used to collect the respective device parameters.

## 2. Synthetic Details

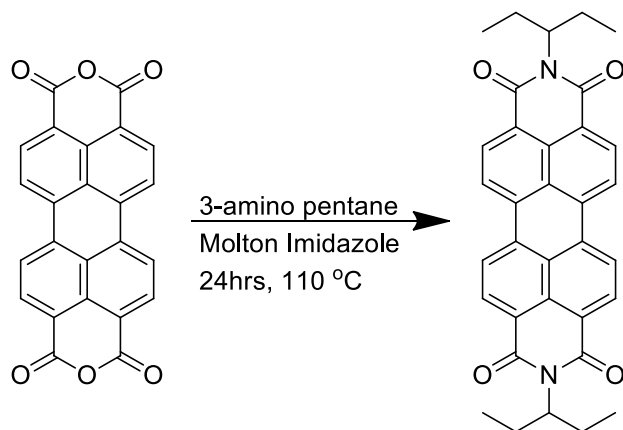
### Materials Synthesis

For a direct comparison, both the target monomers and dimers were synthesized with C5 (3-pentyl) alkyl groups at the imide position, branching at the C3-position. The N-annulated PDI materials were synthesized with hexyl alkyl groups at the pyrrole nitrogen position. The N-annulated PDI monomer (**2**) and dimer (**4**) were both synthesized using our previously reported synthesis.<sup>52</sup> The non-annulated dimer **3** was synthesized in three steps, full experimental details can be found in the supplementary information (SI). The first step followed a previously reported synthetic procedure to produce PDI **1** in a yield of 90%.<sup>1,2</sup> Bromination of compound **1** to give compound **6** was achieved using elemental bromine in under 30 minutes. An issue is that the addition of Br is not stepwise or selective leading to multiple Br containing products. This issue has been well documented.<sup>3-5</sup> Separation is accomplished using silica-gel column chromatography to give analytically pure **6** (45% yield). The target dimer, compound **3**, was synthesized using a modified Negishi coupling of **6**.<sup>1,6</sup> Unfortunately, yields were low (ca. 20%) owing to significant debromination of the starting material. Comparatively, the N-annulated dimer **4** was synthesized in higher yield with simpler purification (i.e. precipitation versus chromatography) than the non-annulated dimer **3**. Newly synthesized compound **3**, was characterized by <sup>1</sup>H and <sup>13</sup>C NMR spectroscopy and mass spectrometry.



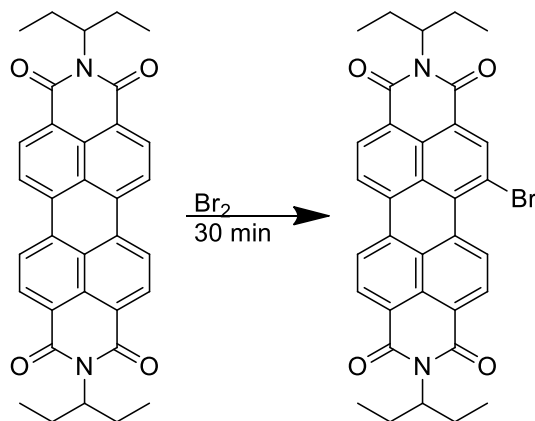
**Scheme 1.** The synthetic pathway towards the PDI Materials **1**, **2**, **3**, and **4**.

## Experimental Procedures



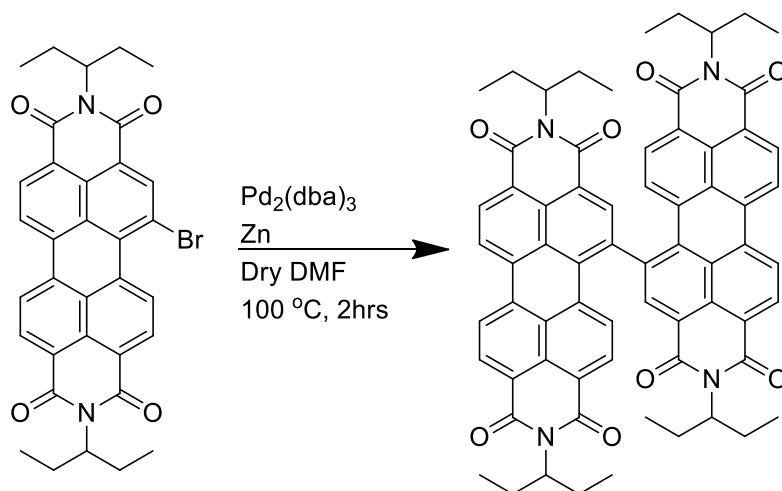
Synthesis of PDI (1).

**Synthesis of PDI (1):** Synthesis was carried out using previously reported literature procedure.<sup>1,7</sup> Yield was 90% for 18.0g. Spectroscopic data matches previous literature reports.<sup>7</sup>



Synthesis of Br-PDI (6).

**Synthesis of Br-PDI (6):** Synthesis was carried out with a modified previously reported literature procedure.<sup>8,9</sup> PDI (2.24g,  $4.22 \times 10^{-3}$  mol) was added to 250 mL round bottom flask containing a stir bar. Neat Br<sub>2</sub> (6.0 mL,  $1.17 \times 10^{-1}$  mol) was added via syringe to the round bottom flask. The reaction proceeded while stirring for 30 min. A saturated Na<sub>2</sub>SO<sub>3</sub> solution was added to the reaction mixture very slowly at the 27 minute mark so the reaction would be quenched by the 30-minute mark. The reaction mixture was filtered and washed with approximately 150 mL of water. A red solid was isolated which was purified by silica gel column chromatography in dichloromethane. Product elutes as the second spot on TLC. Isolated product is a bright red solid. The yield was 45% for 1.17 g. Spectroscopic data matches previous literature reports.<sup>8</sup>



Synthesis of tPDI<sub>2</sub> (3).

**Synthesis of tPDI<sub>2</sub> (3):** Synthesis was carried out using a modified literature procedure.<sup>1</sup> Compound **6** (167 mg, 2.73\*10<sup>-3</sup> mol) and Zn dust (43 mg, 6.57\*10<sup>-3</sup> mol) were added to a 20 mL microwave vial with a stir bar and was dried in a vacuum oven at 80 °C overnight. Pd<sub>2</sub>(dba)<sub>3</sub> (22 mg, 16 mol% loading) was added in the glovebox and the vial was sealed in the glovebox. Dry DMF (4 mL) was added via syringe. The reaction mixture was heated while stirring at 100 °C for 2 hours. TLC analysis indicated complete starting material consumption. The reaction mixture was poured into 15 mL of dichloromethane. The mixture was poured through a silica gel pad to remove catalyst and zinc and the solution was removed in vacuo to produce a dark red solid. TLC analysis indicated debrominated starting material, product, and two other compounds. The crude solid material was purified by silica gel column chromatography with a gradient of 20% acetone in hexanes. The solvent was removed in vacuo and yielded a dark red solid. The red solid was then further purified by recrystallization in acetone layered in hexanes (1:9) and left overnight in the freezer. The solvent was decanted, and the precipitate was dried further in vacuo. Solid was removed from the round bottom with a 1:1 mixture of water:MeOH and filtered in a Hirsch funnel which produced a dark red solid (29 mg). The solid was dried in a vacuum oven at 80 °C overnight to remove residual solvent. The product yield was 20%.

**<sup>1</sup>H NMR (500 MHz, CDCl<sub>3</sub>):** δ 8.84 – 8.77 (m, 8H), 8.50 (d, *J* = 8.3 Hz, 2H), 8.18 (d, *J* = 9.6 Hz, 4H), 5.08 – 4.90 (m, 4H), 2.29 – 2.09 (m, 8H), 1.96 – 1.77 (m, 8H), 1.02 – 0.71 (m, 24H).

**<sup>13</sup>C{<sup>1</sup>H} NMR (126 MHz, CDCl<sub>3</sub>):** δ 142.02, 134.96, 134.37, 134.22, 133.08, 129.75, 129.02, 128.90, 127.62, 127.51, 124.17, 123.57, 58.03, 57.85, 25.10, 11.42.

**HRMS:** Calculated 1058.43. Found 1058.4282



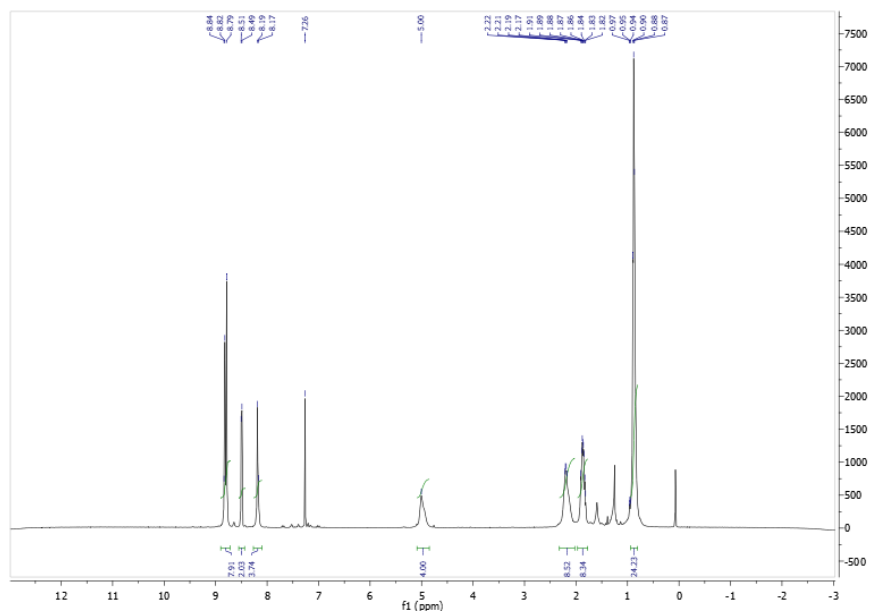


**Figure S3)**  $^1\text{H}$  NMR spectrum of **3** in  $\text{CDCl}_3$ .

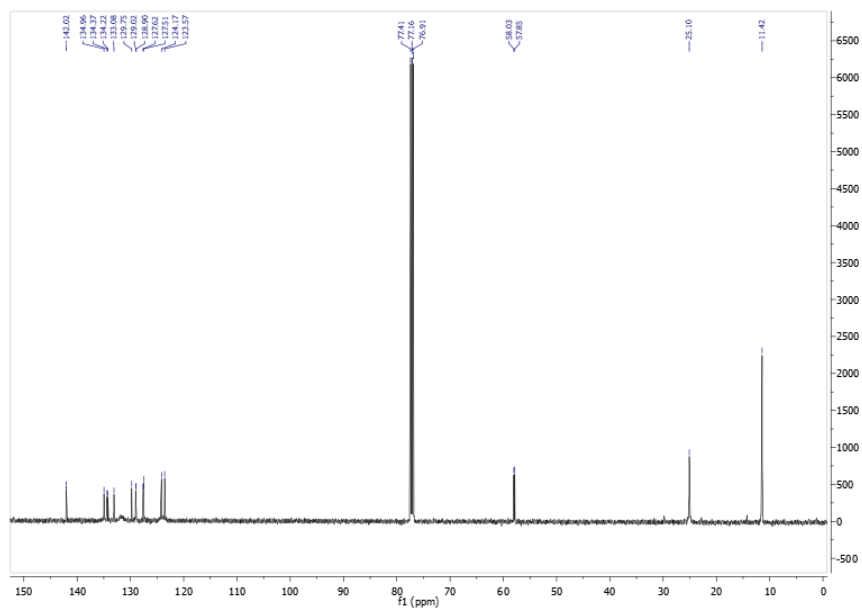


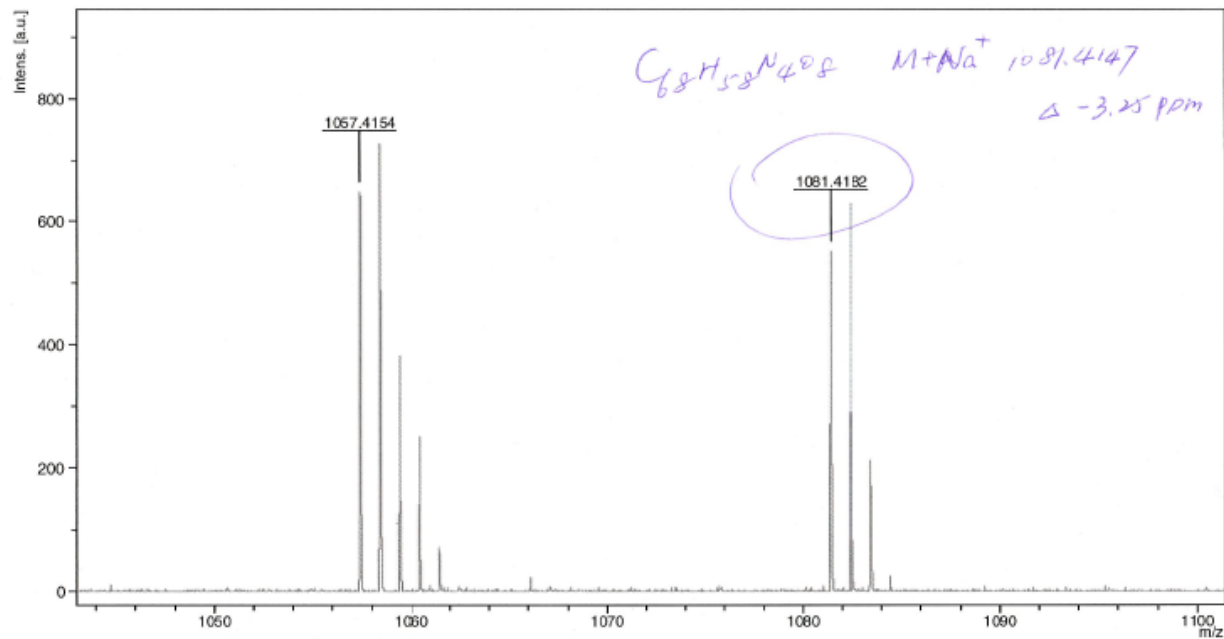
**Figure S4)**  $^{13}\text{C}$   $\{^1\text{H}\}$  NMR spectrum of **3** in  $\text{CDCl}_3$ .

## 4. High-Resolution Mass Spectrometry

D:\Data\2018\012018\GW180126EC1.N13.HCCA\0\_N13\1

Comment 1 EDWARD/EC-33/1058/HCCA

Comment 2



Bruker Daltonics flexAnalysis

printed: 1/26/2018 9:25:53 AM

Figure S5) High-resolution mass spectrum of **3**.

## 5. Temperature Dependent Optical Absorption Spectra of Neat Compounds

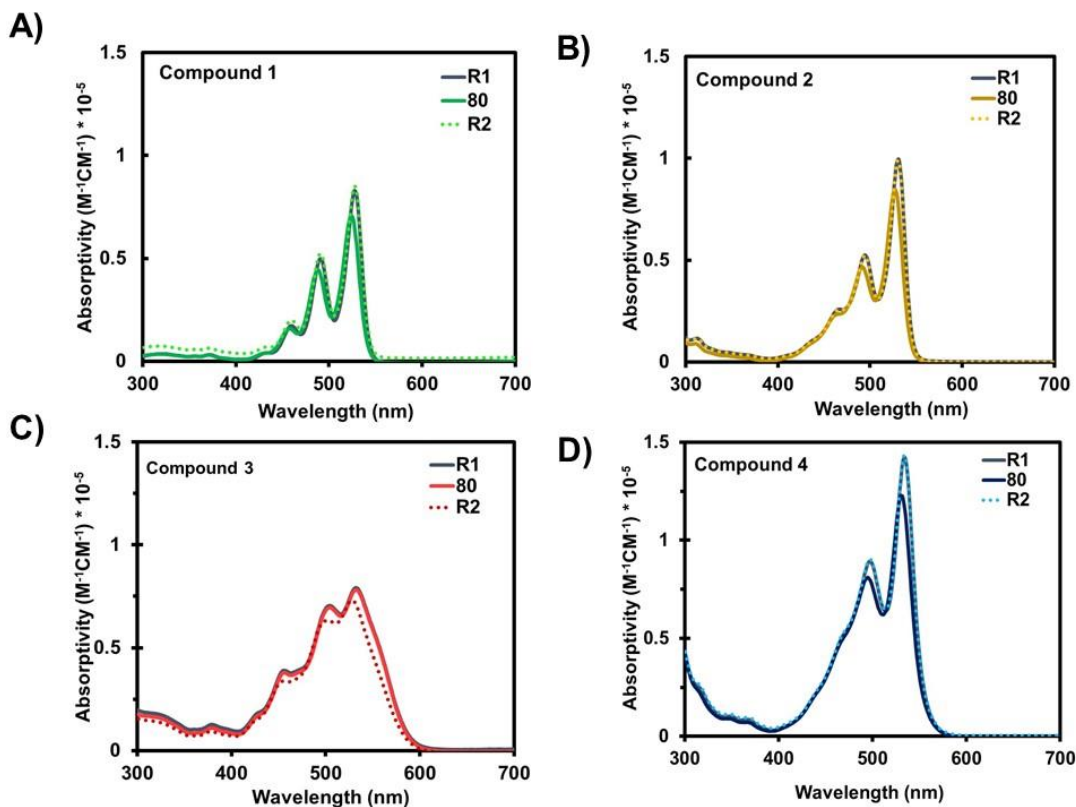


**Figure S6.** UV-visible spectra of compounds A) **1**, B) **2**, C) **3**, and D) **4** in  $C_6H_5Cl$  in room temperature (R1), heated to 80 °C, and cooled down to room temperature (R2).

## 6. Photoluminescence Spectra of Neat Compounds

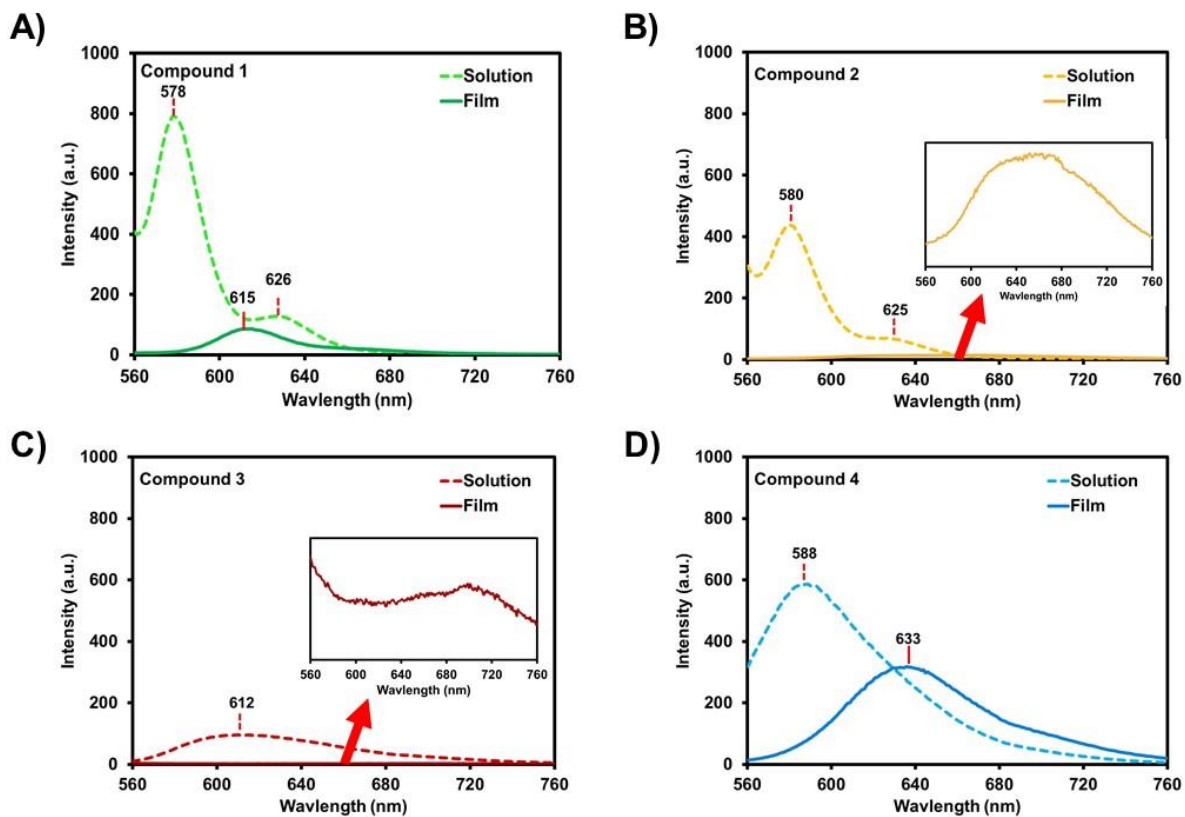


**Figure S7.** Photoluminescence spectra of PDI materials A) 1, B) 2, C) 3, and D) 4 in  $C_6H_5Cl$  and as 'as-cast' films spin-coated from  $C_6H_5Cl$  solutions. A zoomed-in image of photoluminescence spectra of the films of compound 2 and 3 are inserted.

## 7. Electrochemistry

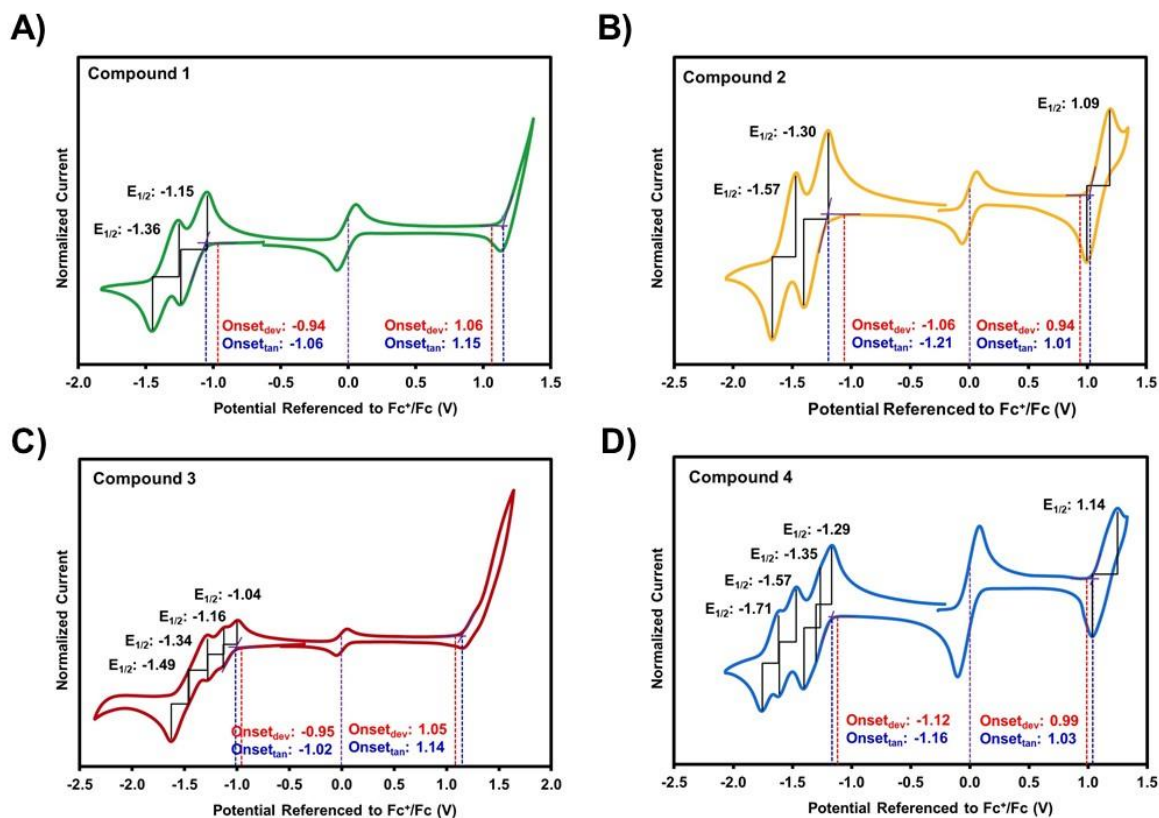


**Figure S8.** Cyclic voltammograms (with ferrocene internal standard) of compounds A) **1**, B) **2**, C) **3**, and D) **4** with onset potentials and E<sub>1/2</sub> values shown. This figure is different from Figure 4 in that the full positive scans for compounds **1** and **3** are shown.

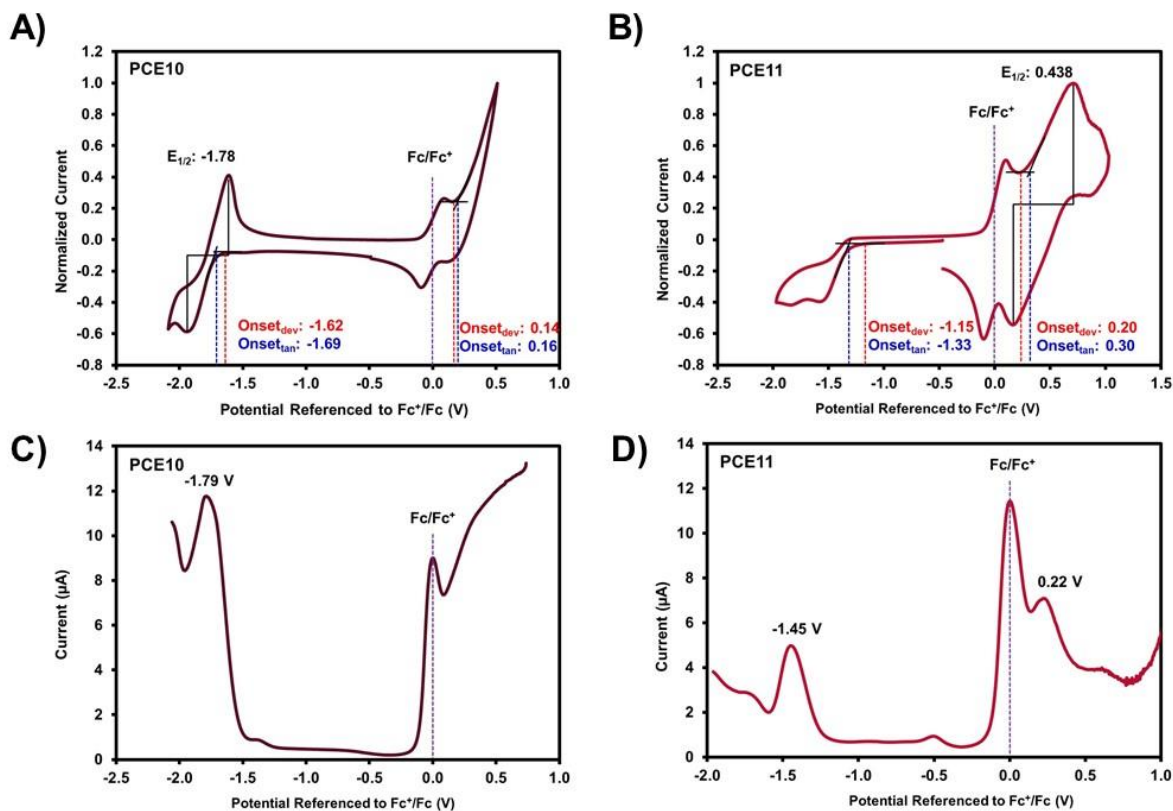


**Figure S9.** Cyclic voltammograms of **A)** PTB7-Th (PCE10) and **B)** PffBT4T-2OD (PCE11) with onset potentials and  $E_{1/2}$  values shown and differential pulse voltammograms of **C)** PTB7-Th (PCE10) and **D)** PffBT4T-2OD (PCE11) with peak potentials shown.

## 8. Computational Analysis

DFT calculations can often provide insights into experimental data such as photophysical properties, energy levels, or molecular geometry.<sup>10-12</sup> For this study, optimized geometry calculations were performed for compounds **1**, **2**, **3**, and **4**<sup>52</sup> using the B3LYP<sup>13-15</sup> level of theory with 6-31G(d,p)<sup>16-21</sup> basis set. From the optimized geometries, TD-SCF<sup>22</sup> calculations were performed to generate molecular orbital representations and simulated absorption spectra. These calculations were done to determine theoretical energy levels and simulated absorption profiles and compare them with the experimentally determined IP and EA and absorption spectra. The results are displayed in Figure S11 and the summary of predicted optical transitions and oscillator strengths is shown in Table S1.

The theoretical HOMO and LUMO energy levels follow the same trend as was experimentally determined from electrochemical measurements, where the N-annulated compounds **2** and **4** have raised HOMO and LUMO energy levels compared to their non-annulated counterparts **1** and **3**, respectively. N-annulation results in significant changes to the molecular orbitals. For instance, in compound **1** the HOMO-2 and HOMO-1 are degenerate and are localized at the imide groups of the molecule. Compound **2** has a similar HOMO-2 as **1** but the HOMO-1 is now occupying the core of the molecule with significant contribution from the pyrrole-N, making it higher energy than the HOMO-1 of **1**. The LUMO of **2** also has a pyrrole-N contribution. In **4**, the pyrrole-N contributes to the HOMO-2, making it significantly higher energy than **3**'s HOMO-2, while the HOMO-1 and HOMO of **4** are nearly degenerate, like **3**. The LUMO and LUMO+1 of **4** also both have a contribution from the pyrrole-N. The theoretical band gaps are slightly higher by 0.1 to 0.4 eV than experimental band gaps, but this is to be expected. Since calculations are based on a single molecule in the gas phase while experimental results are based on a bulk sample in solution, a larger calculated band gap than experimentally determined is typical. This is also reflected in the simulated absorption spectra (Figure 5C), where theoretical absorption maxima are blue-shifted compared to the experimental results.

Except for compound **3**, all compounds show very similar simulated absorption spectra. The monomer compounds **1** and **2** both show only one HOMO–LUMO transition. Compound **3** shows a significant red-shifted shoulder in the spectrum due to the HOMO–LUMO transition, while the main portion of the spectrum is accounted for by the HOMO-1–LUMO and HOMO-1–LUMO+1 transitions. Compound **4** lacks a HOMO–LUMO transition and instead the spectrum is dominated by HOMO–LUMO+1, HOMO-1–LUMO+1, and HOMO-2–LUMO transitions. Why only compound **3** shows this red-shifted shoulder is unclear. This difference is reflected in the experimental results, where the absorption profile of **3** in solution was significantly broadened with less distinct peaks compared to the absorption profiles of the other compounds. Despite this irregularity in the simulated optical spectra, the theoretical calculations correlate well with the experimental electrochemistry results.

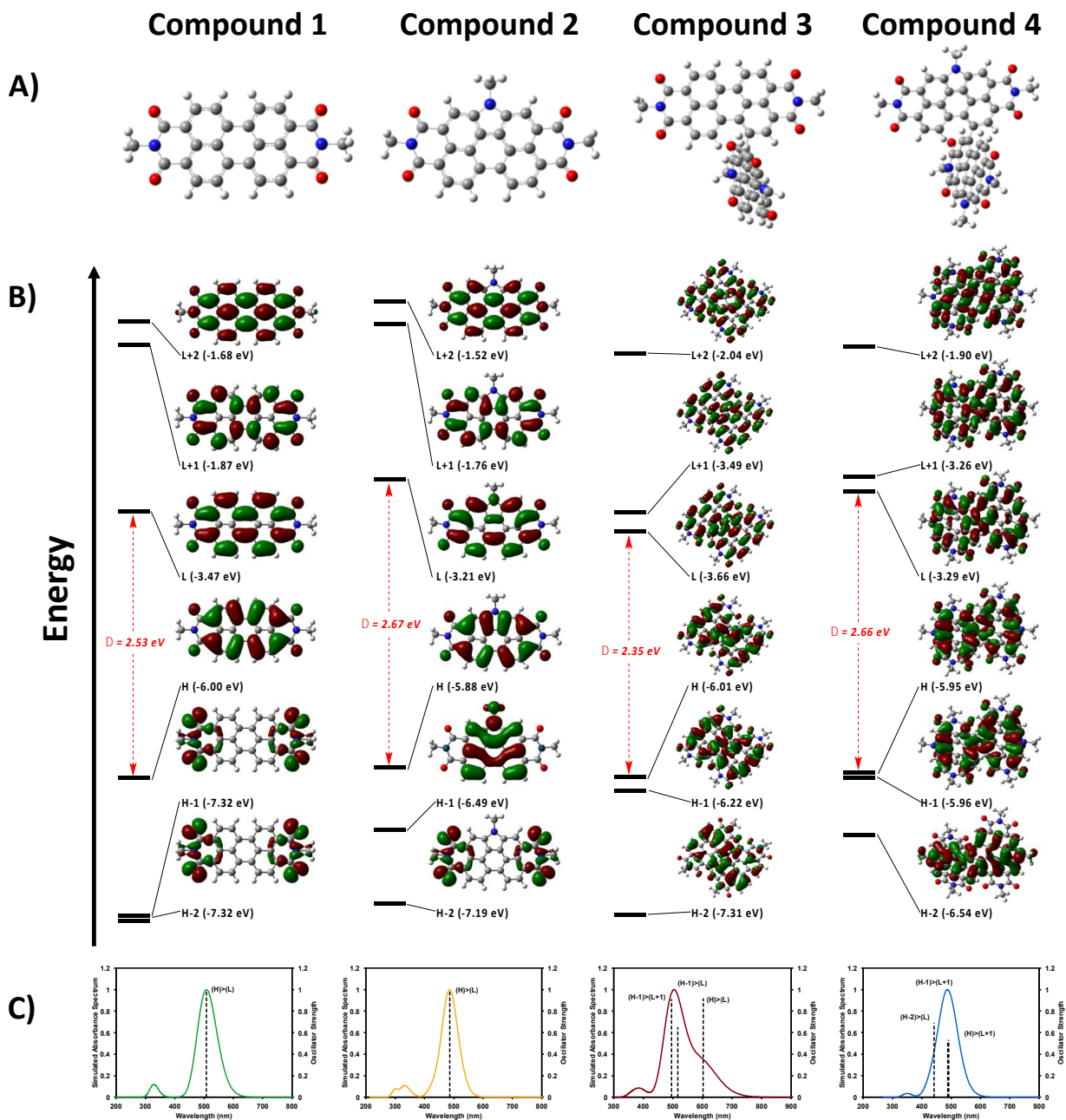


**Figure S10.** A) Optimized geometry for PDI materials **1**, **2**, **3**, and **4**. B) Calculated electronic energy levels and energy gaps. C) Calculated optical absorption profiles with oscillator strengths shown. Calculations were done on Gaussian09,<sup>23</sup> input files and results were visualized using GausView05.<sup>24</sup> All alkyl chains were replaced with a methyl group. The B3LYP<sup>13–15</sup> level of theory with 6-31G(d,p)<sup>16–21</sup> basis set were used for the calculations. TD-SCF<sup>22</sup> calculations were performed from the optimized geometry. The single point calculation was performed on this structure to generate molecular orbitals and electrostatic potential maps.

**Table S1.** Summary of predicted optical transitions from TD-DFT calculations.

Compound	State	$E_{\text{opt}}$ (eV)	$\lambda$ (nm)	f	Composition
<b>1</b>	S <sub>1</sub>	2.44	508	0.666	H → L (100%)
<b>2</b>	S <sub>1</sub>	2.55	486	0.606	H → L (98%)
<b>3</b>	S <sub>1</sub>	2.06	602	0.262	H → L (92%) H-1 → L+1 (8%)
	S <sub>3</sub>	2.40	516	0.108	H-1 → L (65%) H → L+1 (35%)
	S <sub>4</sub>	2.50	495	0.577	H-1 → L+1 (91%) H → L (8%)
<b>4</b>	S <sub>3</sub>	2.52	492	0.587	H → L+1 (53%) H-1 → L (44%)
	S <sub>4</sub>	2.54	488	0.496	H-1 → L+1 (52%) H → L (45%)
	S <sub>5</sub>	2.81	442	0.228	H-2 → L (69%) H-3 → L+1 (26%)

## 9. Optical Absorption and Photoluminescence Spectroscopy of BHJ Films

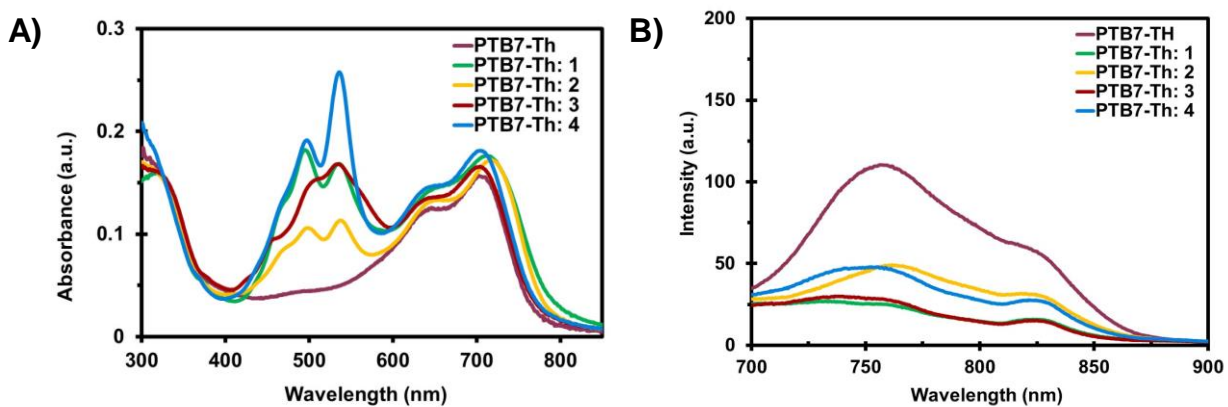


**Figure S11.** A) Optical absorption spectra and B) Photoluminescence spectra of PTB7-Th film and PTB7-Th blended (with PDI NFA) films cast from  $C_6H_5Cl$ .

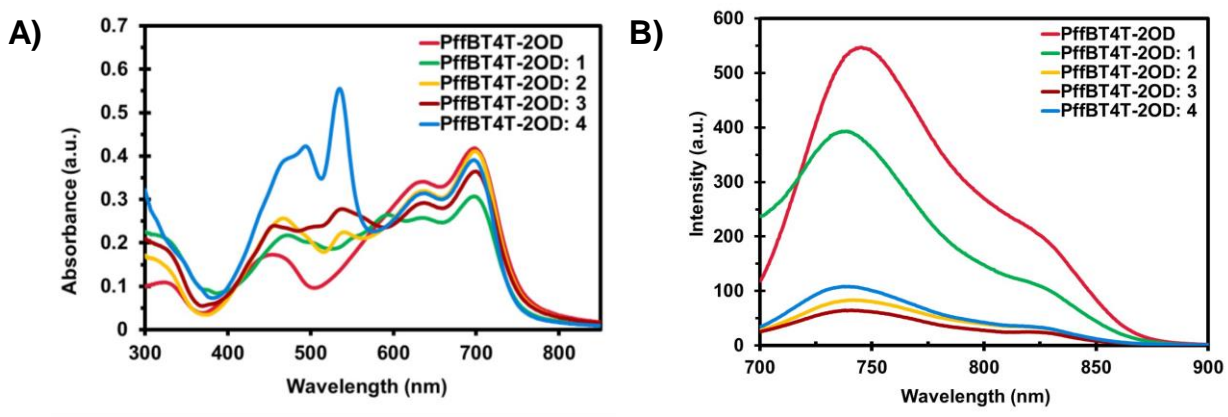


**Figure S12.** A) Optical absorption spectra and B) Photoluminescence spectra of PffBT4T-2OD film and PffBT4T-2OD blended (with PDI NFA) films cast from  $C_6H_5Cl$ .

## 10. Organic Solar Cells Data

**OSC Fabrication and Testing:** Devices were fabricated using ITO-coated glass substrates cleaned by sequentially ultra-sonicating detergent and de-ionized water, acetone, and isopropanol followed by exposure to UV/ozone for 30 minutes. ZnO was subsequently deposited as a sol-gel precursor solution in the air following the method of Sun et al.<sup>25</sup>. The room temperature solution was filtered and spun-cast at a speed of 4000 rpm and then annealed at 200 °C in air for 15 min. Solutions of PTB7-Th (CAL-OS, PCE10, Mw > 100 kg/mol, batch no C-03), PffBT4T-2OD (1- Material, PCE11, Mw = 100-150 kg/mol, PDI=2.0-2.5, batch no YY8198CB), and compounds **1**, **2**, **3**, and **4** were prepared in air with a total concentration of 10 mg/mL in C<sub>6</sub>H<sub>5</sub>Cl, stirred, then mixed to create the spin-casting blend solutions.

Solutions of compound **1** were stirred and heated for only 1 h at 70 °C, further time lead to precipitation. Solutions of PTB7-Th and compounds **2** and **3** were stirred at 70 °C for 4-6 h to ensure full dissolution. Solutions of compound **4** were stirred and heated for 1 h at 70 °C, although the compound readily dissolved at room temperature. Solutions of PffBT4T-2OD were stirred at 110 °C for at least 3 h to ensure full dissolution.

Equal part aliquots of each neat solution were taken and combined to give the spin-casting blend solutions with a 1:1 by weight ratio of active materials with a total 10 mg/mL solution concentration. Blend solutions using PTB7-Th polymer were stirred at 70 °C for 1 hour, allowed to cool to room temperature, then spin-coated onto the ITO/ZnO substrates at 1500 rpm. Blend solutions using PffBT4T-2OD polymer were stirred at 110 °C for 1 hour, then immediately hot spin-casted onto the ITO/ZnO substrates at 1200 rpm.

All layered films were kept in an N<sub>2</sub> atmosphere glovebox overnight before evaporating MoO<sub>3</sub> and Ag. Films of MoO<sub>3</sub> (10 nm) followed by Ag (100 nm) were thermally deposited under vacuum (3x10<sup>-6</sup> Torr). The active areas of resulting devices were 0.09 cm<sup>2</sup>.

**Table S2.** Organic solar cell data of the PTB7-Th:PDI blends (1:1) cast from chlorobenzene. Best results are highlighted in bold. Averages are in italics.

blend	V <sub>oc</sub> (V)	J <sub>sc</sub> (mA/cm <sup>2</sup> )	FF (%)	PCE (%)
<b>PTB7-Th:1</b>	0.81	9.48	39.36	3.03
	0.81	9.47	38.91	2.98
	0.81	10.77	43.27	3.79
	0.73	9.76	36.70	2.62
	0.79	11.49	41.61	3.79
	<b>0.81</b>	<b>11.51</b>	<b>43.20</b>	<b>4.01</b>
	<i>0.81</i>	<i>10.30</i>	<i>40.79</i>	<i>3.40</i>
<b>PTB7-Th:2</b>	0.97	7.06	31.98	2.18
	0.98	7.03	33.64	2.31
	1.00	7.38	35.08	2.60
	1.04	6.84	32.14	2.28
	1.01	7.42	33.58	2.52
	1.01	6.94	33.71	2.37
	1.01	7.44	33.93	2.54
	<b>1.00</b>	<b>7.56</b>	<b>34.17</b>	<b>2.60</b>
	0.88	6.09	31.77	1.71
	0.87	6.19	32.93	1.78
	1.03	6.79	32.45	2.26
	1.00	6.79	33.56	2.28
	<i>0.98</i>	<i>6.96</i>	<i>33.25</i>	<i>2.29</i>
<b>PTB7-Th:3</b>	<b>0.75</b>	<b>10.41</b>	<b>52.25</b>	<b>4.07</b>
	0.73	9.81	53.25	3.83
	0.69	10.61	52.20	3.84
	0.74	10.26	48.66	3.70
	<i>0.73</i>	<i>10.27</i>	<i>51.59</i>	<i>3.86</i>
<b>PTB7-Th:4</b>	0.96	11.83	46.42	5.28
	<b>0.99</b>	<b>12.37</b>	<b>46.91</b>	<b>5.72</b>
	0.98	12.31	47.08	5.67
	0.97	11.69	48.06	5.47
	0.98	11.45	49.01	5.47
	0.96	12.48	45.46	5.44
	0.97	12.47	45.21	5.48
	<i>0.97</i>	<i>12.09</i>	<i>46.88</i>	<i>5.51</i>

**Table S3.** Organic solar cell data of the PffBT4T-2OD:PDI blends (1:1) cast from chlorobenzene. Best results are highlighted in bold. Averages are in italics.

blend	V <sub>oc</sub> (V)	J <sub>sc</sub> (mA/cm <sup>2</sup> )	FF (%)	PCE (%)
<b>PffBT4T-2OD:1</b>	0.79	3.68	42.50	1.23
	0.72	3.49	35.25	0.89
	<b>0.80</b>	<b>4.46</b>	<b>44.28</b>	<b>1.59</b>
	0.80	3.66	44.43	1.31
	<i>0.78</i>	<i>3.82</i>	<i>41.62</i>	<i>1.25</i>
<b>PffBT4T-2OD:2</b>	0.91	3.50	37.67	1.20
	<b>0.98</b>	<b>4.03</b>	<b>42.95</b>	<b>1.69</b>
	0.95	3.59	42.79	1.47
	<i>0.95</i>	<i>3.71</i>	<i>41.13</i>	<i>1.45</i>
<b>PffBT4T-2OD:3</b>	<b>0.79</b>	<b>9.77</b>	<b>47.37</b>	<b>3.66</b>
	0.78	9.51	47.43	3.50
	0.79	9.65	47.92	3.65
	0.78	9.56	47.96	3.56
	<i>0.78</i>	<i>9.62</i>	<i>47.67</i>	<i>3.59</i>
<b>PffBT4T-2OD:4</b>	1.02	7.23	40.07	2.95
	1.02	7.51	41.61	3.19
	1.00	7.18	40.18	2.89
	<b>1.02</b>	<b>8.32</b>	<b>42.13</b>	<b>3.59</b>
	1.01	7.80	42.08	3.32
	1.02	7.45	40.51	3.09
	1.01	6.96	37.92	2.67
	1.03	7.34	43.01	3.24
	1.01	7.26	42.39	3.11
	1.02	7.10	40.85	2.97
	1.01	6.57	39.21	2.60
	<i>1.02</i>	<i>7.34</i>	<i>40.91</i>	<i>3.06</i>

## 11. AFM Height and Phase Images of BHJ Blends

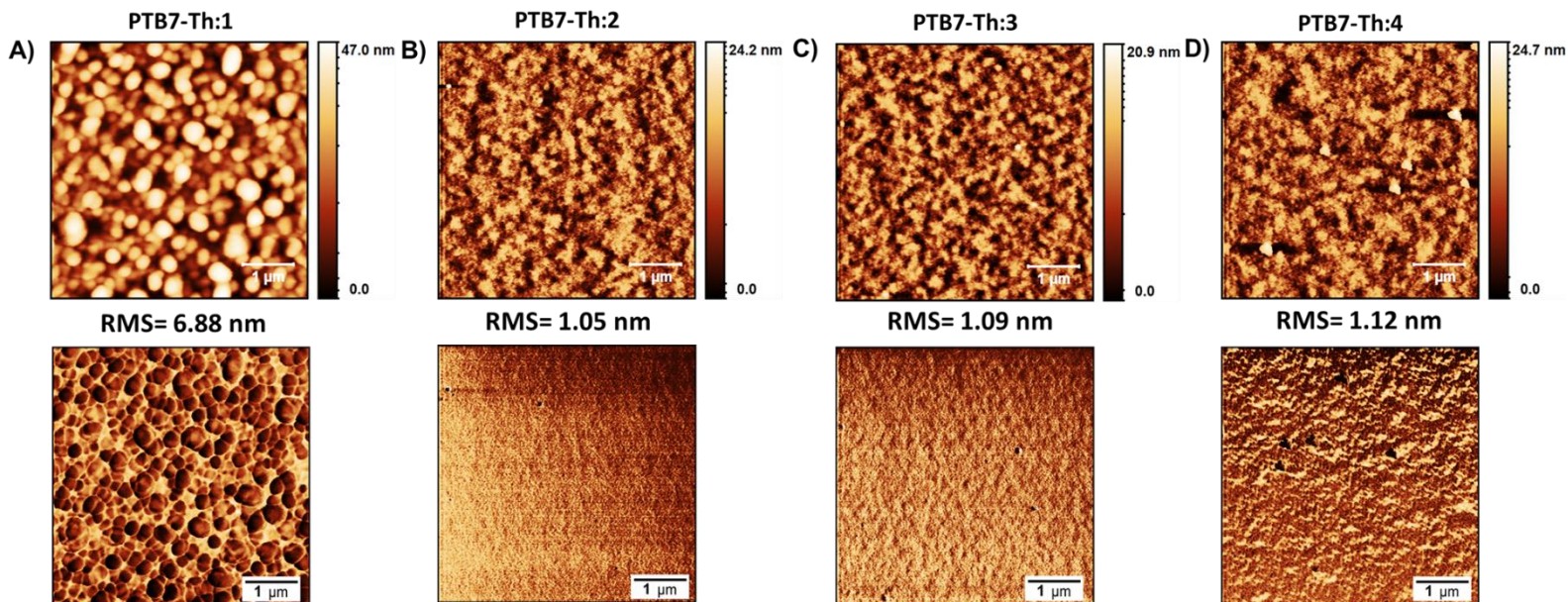


**Figure S13.** AFM height (top) and phase (bottom) images for PffBT4T-2OD based BHJ organic solar cells. A) PTB7-Th :1 B) PTB7-Th:2 C) PTB7-Th :3 D) PTB7-Th:4

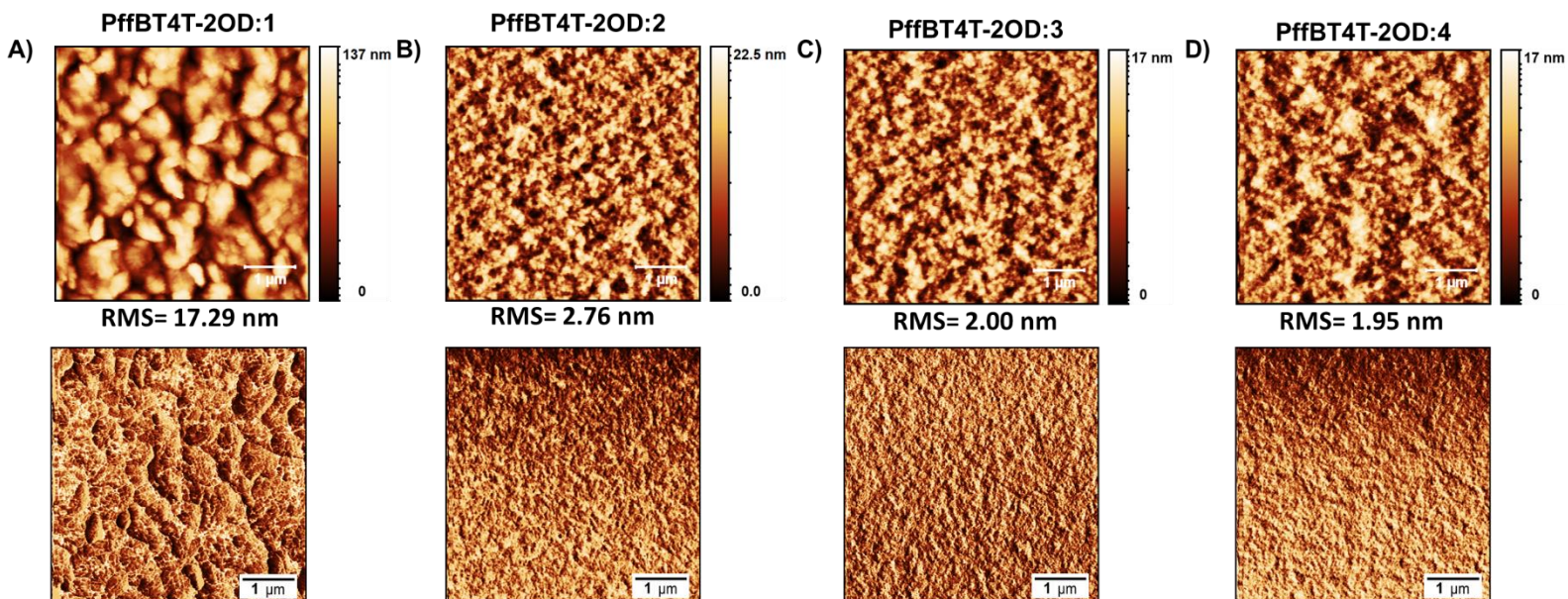


**Figure S14.** AFM height (top) and phase (bottom) images for PffBT4T-2OD based BHJ organic solar cells. A) PffBT4T-2OD:1 B) PffBT4T-2OD:2 C) PffBT4T-2OD:3 D) PffBT4T-2OD:4

## 12. References

- (1) Hendsbee, A. D.; Sun, J. P.; Law, W. K.; Yan, H.; Hill, I. G.; Spasyuk, D. M.; Welch, G. C. Synthesis, Self-Assembly, and Solar Cell Performance of N-Annulated Perylene Diimide Non-Fullerene Acceptors. *Chem. Mater.* **2016**, *28* (19), 7098–7109. <https://doi.org/10.1021/acs.chemmater.6b03292>.
- (2) Demmig, S.; Langhals, H. Leichtlösliche, Lichtechte Perylen-Fluoreszenzfarbstoffe. *Chem. Ber.* **1988**, *121* (2), 225–230. <https://doi.org/10.1002/cber.19881210205>.
- (3) Cohen, E.; Weissman, H.; Shimoni, E.; Kaplan-Ashiri, I.; Werle, K.; Wohlleben, W.; Rybtchinski, B. Robust Aqua Material: A Pressure-Resistant Self-Assembled Membrane for Water Purification. *Angew. Chem. Int. Ed.* **2017**, *56* (8), 2203–2207. <https://doi.org/10.1002/anie.201610288>.
- (4) Hendsbee, A. D.; McAfee, S. M.; Sun, J.-P.; McCormick, T. M.; Hill, I. G.; Welch, G. C. Phthalimide-Based  $\pi$ -Conjugated Small Molecules with Tailored Electronic Energy Levels for Use as Acceptors in Organic Solar Cells. *J. Mater. Chem. C* **2015**, *3* (34), 8904–8915. <https://doi.org/10.1039/C5TC01877C>.
- (5) Yang, Y.; Wang, Y.; Xie, Y.; Xiong, T.; Yuan, Z.; Zhang, Y.; Qian, S.; Xiao, Y. Fused Perylenebisimide–Carbazole: New Ladder Chromophores with Enhanced Third-Order Nonlinear Optical Activities. *Chem. Commun.* **2011**, *47* (38), 10749. <https://doi.org/10.1039/c1cc14071j>.
- (6) Welch, G. C.; Vespa, M.; Cann, J.; Dayneko, S.; Melville, O.; Hendsbee, A.; Lessard, B.; Zhou, Y. Synthesis of a Perylene Diimide Dimer with Pyrrolic N-H Bonds and N-Functionalized Derivatives for Organic Field-Effect Transistors and Organic Solar Cells. *Eur. J. Org. Chem.* **2018**. <https://doi.org/10.1002/ejoc.201801055>.
- (7) Demmig, S.; Langhals, H. Leichtlösliche, Lichtechte Perylen-Fluoreszenzfarbstoffe. *Chem Ber* **1988**, *121* (2), 225–230.
- (8) Rajasingh, P.; Cohen, R.; Shirman, E.; Shimon, L. J. W.; Rybtchinski, B. Selective Bromination of Perylene Diimides under Mild Conditions. *J. Org. Chem.* **2007**, *72* (16), 5973–5979. <https://doi.org/10.1021/jo070367n>.
- (9) Cohen, E.; Weissman, H.; Shimoni, E.; Kaplan-Ashiri, I.; Werle, K.; Wohlleben, W.; Rybtchinski, B. Robust Aqua Material: A Pressure-Resistant Self-Assembled Membrane for Water Purification. *Angew. Chem. - Int. Ed.* **2017**, *56* (8), 2203–2207. <https://doi.org/10.1002/anie.201610288>.
- (10) Rutledge, L. R.; McAfee, S. M.; Welch, G. C. Design and Computational Characterization of Non-Fullerene Acceptors for Use in Solution-Processable Solar Cells. *J. Phys. Chem. A* **2014**, *118* (36), 7939–7951. <https://doi.org/10.1021/jp505867y>.
- (11) Jiang, W.; Xiao, C.; Hao, L.; Wang, Z.; Ceymann, H.; Lambert, C.; Di Motta, S.; Negri, F. Localization/Delocalization of Charges in Bay-Linked Perylene Bisimides. *Chem. - Eur. J.* **2012**, *18* (22), 6764–6775. <https://doi.org/10.1002/chem.201103954>.
- (12) Yin, H.; Geng, Y.; Sun, G.-Y.; Su, Z.-M. Theoretical Design of Perylene Diimide Dimers with Different Linkers and Bridged Positions as Promising Non-Fullerene Acceptors for Organic

- Photovoltaic Cells. *J. Phys. Chem. C* **2017**, *121* (4), 2125–2134. <https://doi.org/10.1021/acs.jpcc.6b12174>.
- (13) Becke, a. D. Density-Functional Exchange-Energy Approximation with Correct Asymptotic Behavior. *Phys. Rev. A* **1988**, *38* (6), 3098–3100. <https://doi.org/DOI:10.1103/PhysRevA.38.3098>.
- (14) Lee, C.; Yang, W.; Parr, R. Development of the Colle- Salvetti Correlation Energy Formula into a Functional of the Electron Density. *Phys Rev B* **1988**, *37* (2), 785–789. <https://doi.org/DOI:10.1103/PhysRevB.37.785>.
- (15) Miehlich, B.; Savin, A.; Stoll, H.; Preuss, H. Results Obtained with the Correlation Energy Density Functionals of Becke and Lee, Yang and Parr. *Chem. Phys. Lett.* **1989**, *157* (3), 200–206. [https://doi.org/10.1016/0009-2614\(89\)87234-3](https://doi.org/10.1016/0009-2614(89)87234-3).
- (16) Hehre, W. J.; Pople, R. D. and J. A. Self—Consistent Molecular Orbital Methods. XII. Further Extensions of Gaussian—Type Basis Sets for Use in Molecular Orbital Studies of Organic Molecules. *J. Chem. Phys.* **1972**, *56* (5), 2257–2261. <https://doi.org/http://dx.doi.org/10.1063/1.1677527>.
- (17) Hariharan, P. C.; Pople, J. A. The Influence of Polarization Functions on Molecular Orbital Hydrogenation Energies. *Theor. Chim. Acta* **1973**, *28* (3), 213–222. <https://doi.org/10.1007/BF00533485>.
- (18) Francl, M. M.; Pietro, W. J.; Hehre, W. J.; Binkley, J. S.; Gordon, M. S.; Francl, M. M.; Pietro, W. J.; Hehre, W. J.; Binkley, J. S.; Gordon, M. S. Selfconsistent Molecular Orbital Methods . XXIII . A Polarization-type Basis Set for Secondrow Elements Self-Consistent Molecular Orbital Methods . XXIII . A Polarization-Type Basis Set for Second-Row Elements. *J Chem Phys* **1982**, *77* (7), 3654. <https://doi.org/10.1063/1.444267>.
- (19) Binning, R. C.; Curtiss, L. A. Compact Contracted Basis Sets for Third-row Atoms: Ga–Kr. *J. Comput. Chem.* **1990**, *11* (10), 1206–1216. <https://doi.org/10.1002/jcc.540111013>.
- (20) Rassolov, V. A.; Pople, J. A.; Ratner, M. A.; Windus, T. L.; Rassolov, V. A.; Pople, J. A.; Ratner, M. A.; Windus, T. L. 6-31G\* Basis Set for Atoms K through Zn. *J Chem Phys* **2003**, *109* (4), 1223–1229. <https://doi.org/10.1063/1.476673>.
- (21) Rassolov, V. A.; Ratner, M. A.; Pople, J. A.; Redfern, P. C.; Curtiss, L. A. 6-31G\* Basis Set for Third-Row Atoms. *J. Comput. Chem.* **2001**, *22* (9), 976–984. <https://doi.org/10.1002/jcc.1058>.
- (22) Bauernschmitt, R.; Ahlrichs, R. Treatment of Electronic Excitations within the Adiabatic Approximation of Time Dependent Density Functional Theory. *Chem. Phys. Lett.* **1996**, *256* (4–5), 454–464. [https://doi.org/10.1016/0009-2614\(96\)00440-X](https://doi.org/10.1016/0009-2614(96)00440-X).
- (23) Frisch, M.; Trucks, G.; Schlegel, H.; Scuseria, G.; Robb, M.; Cheeseman, J.; Scalmani, G.; Barone, V.; Mennucci, B.; Petersson, G.; et al. Gaussian 09, Revision D.01. *Gaussian 09 Revis. B01 Gaussian Inc Wallingford CT* **2009**.
- (24) Dennington, R.; Keith, T. A.; Millam, J. M. GaussView, Version 5. *Semichem Inc Shawnee Mission KS* **2009**.

- (25) Sun, Y.; Seo, J. H.; Takacs, C. J.; Seifert, J.; Heeger, A. J. Inverted Polymer Solar Cells Integrated with a Low-Temperature-Annealed Sol-Gel-Derived ZnO Film as an Electron Transport Layer. *Adv. Mater.* **2011**, *23* (14), 1679–1683. <https://doi.org/10.1002/adma.201004301>.